

RESEARCH

Open Access



Study on various hot-gas defrosting configurations for CO₂-NH₃ cascade deep freezer

B. S. Arun^{1*}, George Ninan¹, S. Murali¹, Manoj Samuel², Sumit Kumar³, S. Vaishak⁴, Mani Sankar Dasgupta⁴, Sarun Kumar Kochunni⁵, Armin Hafner⁵ and Kristina Norne Widell⁶

Abstract

Four hot-gas bypass defrosting configurations for CO₂-NH₃ cascade blast freezer for application in fish processing firm are numerically investigated. Due to the high moisture content of fish, defrosting is necessary after every 4 to 5 h of batch operation. A thermodynamic model for the cascade system and defrosting was developed to study various defrosting configurations formulated by rearranging the existing compressor to operate as a defrosting compressor and with the addition of an external defrosting compressor. From the simulation findings, it can be summarized that the conventional hot-gas bypass defrosting without defrost compressor is suitable for a high-capacity cascade refrigeration system with more than three evaporators. For low cooling capacity refrigeration systems, a defrosting compressor is necessary to elevate the temperature above the cascade condensing temperature. A dedicated defrosting compressor with a power consumption of 3.1 kW and a modified refrigeration/defrosting compressor with a power consumption of 6.8 kW can deliver 33.3 kW of heating at a temperature of +10 °C (45 bar). Incorporating a desuperheater between the main and defrosting compressors reduces compressor temperature and maintains the lubricating oil stability, without change in defrosting energy consumption and less exergy loss. The defrosting efficiency is obtained in the range of 39.7–42% which is in agreement with published literature.

Keywords Ammonia (R717), Carbon dioxide (R744), Cascade refrigeration, Defrosting, Blast freezer

1 Introduction

Seafood processing industries need various temperatures to maintain the quality of their products. The export of marine products from India stood at 1.39 million metric

tonnes and was valued at USD 6.73 billion during 2018–2019, with an impressive average annual growth rate of about 10% in recent years [1]. After the fresh catch, fish will be stored in a refrigerated chamber or ice chamber in the fishing vessel. Thereafter, it will be transported for deep freezing and stored in cold storages. All this process requires intense refrigeration and high-energy demand, which contributes to carbon emissions. Ammonia has traditionally been used as the refrigerant in these seafood processing industries. With the increase in residential areas around these industries, more people may be affected if there is an ammonia leakage. Moreover, all ammonia systems are space demanding and operate below atmospheric pressure for deep freezing. These efficient, natural refrigerant-based systems are slowly being replaced by synthetic refrigerants having high GWP. However, India's nationally determined contributions (NDCs) to phase out HFCs and restrict the global

*Correspondence:

B. S. Arun
bsarun.indee.cift@gmail.com

¹ Engineering Section, ICAR-Central Institute of Fisheries Technology, Cochin 682029, India

² Centre for Water Resources Development and Management, Kozhikode 673571, India

³ School of Energy Science and Engineering, Indian Institute of Technology, Kharagpur 721302, India

⁴ Department of Mechanical Engineering, Birla Institute of Technology and Science, Pilani 333031, India

⁵ Department of Energy and Process Engineering, Norwegian University of Science and Technology, Trondheim 7034, Norway

⁶ Fisheries and New Biomarine Industry, SINTEF Ocean AS, Trondheim 7465, Norway.



© The Author(s) 2024. **Open Access** This article is licensed under a Creative Commons Attribution 4.0 International License, which permits use, sharing, adaptation, distribution and reproduction in any medium or format, as long as you give appropriate credit to the original author(s) and the source, provide a link to the Creative Commons licence, and indicate if changes were made. The images or other third party material in this article are included in the article's Creative Commons licence, unless indicated otherwise in a credit line to the material. If material is not included in the article's Creative Commons licence and your intended use is not permitted by statutory regulation or exceeds the permitted use, you will need to obtain permission directly from the copyright holder. To view a copy of this licence, visit <http://creativecommons.org/licenses/by/4.0/>.

warming temperature to +2 °C lead to the opportunity adopting CO₂ as a refrigerant. CO₂ has all desirable properties of a good refrigerant such as high vapour density and volumetric capacity for refrigeration. It is non-toxic with A1 safety rating. Ammonia has also excellent properties, but since it is toxic, a viable alternative is to have a cascade system, which limits the filling of ammonia but still utilizes the beneficiary properties.

A complete review of cascade refrigeration systems was presented by M. Pan et al. [2]. These systems can achieve an evaporating temperature as low as -170 °C and have important applications in rapid freezing. The performance of cascade refrigeration system increases with the increase in evaporator temperature, decrease in the condenser outlet temperature (ambient) and maintaining small temperature difference in the cascade heat exchanger. Compared to single-stage and two-stage ammonia refrigeration system, CO₂-NH₃ cascade system is more efficient for very low evaporating temperatures [3]. Various research has been carried out on CO₂-NH₃ cascade refrigeration systems, where NH₃ and CO₂ are used in high-temperature and low-temperature circuit respectively. Lee et al. [4] and Getu and Bansal [5] carried out thermodynamic analyses of CO₂-NH₃ cascade system and determined the optimal cascade condensing temperature for maximum COP, which depends on evaporating temperature, condensing temperature and cascade heat exchanger temperature differences. Alberto Dopazo et al. [6] theoretically analysed a CO₂-NH₃ cascade system for a low-temperature application. They developed relevant correlations to serve as guidelines for the design and optimization of a cascade system. Bingming et al. [3] and Dopazo and Fernandez-seara [7] experimentally investigated the performance of CO₂-NH₃ cascade system. The system was compared with two-stage NH₃ and single-stage NH₃ systems. They found that below -40 °C evaporator temperature, COP of the cascade system is superior to others. Yilmaz et al. [8] conducted a parametric study on CO₂-NH₃ cascade system for different operating and ambient conditions. The maximum COP was found in the range of 1.23–2.37. Bellos and Tzivanidis [9] conducted a comparative study of 18 different CO₂ cascade systems for yearly operation in weather conditions of Athen, Greece. The result showed that natural refrigerants such as NH₃, R290, R600 and R1270 are more appropriate choices according to the energy efficiency and total equivalent warming impact criteria. Saini et al. [10] carried out a comparative analysis of three CO₂-NH₃ cascade system configurations for application in seafood processing for high ambient conditions. The application involved cooling demand in deep freezing and cold storage. For these improved

configurations, they have reported a COP advantage of 11.5–20.3% more than the conventional cascade system.

The deep freezer operating at -40 °C used in the fish processing is susceptible to frost formation on the surface of evaporators because of the high moisture content of fish. The frost build-up on the evaporator reduces the heat transfer effectiveness; therefore, periodic defrosting is required for the freezers. For a batch process such as in blast and plate freezers, the evaporators have to go through defrost within 4 to 5 h, and for a continuous process such as in tunnel and spiral freezers, it requires defrost after 8 to 12 h of operation. Various defrosting methods used are time-off defrost (water spray/air circulation defrost), electric defrost and hot-gas bypass defrost. J. Klingebiel et al. [11] have experimentally compared three commonly applied defrosting methods such as reverse cycle defrosting, electric heating defrosting and warm brine defrosting and concluded that the efficiency of electric heating defrosting is low and warm brine defrosting incurs high equipment costs. Generally, hot-gas bypass defrosting is considered economical and efficient [11, 12]. However, the hot-gas defrosting method, which is commonly followed in industrial refrigeration systems, cannot be directly adopted in case of cascade refrigeration.

1.1 Hot-gas bypass defrosting

In the hot-gas bypass defrosting method, hot gas from the compressor discharge is redirected to the evaporator. It is generally passed through the outlet of the evaporator in the reverse direction [13]. Hereafter, the hot vapour CO₂ condenses inside the evaporator tube and consequently heats the surface of the tube, which results in melting of the frost. The evaporator becomes a condenser during defrosting. Finally, the condensed CO₂ will be collected in the low-pressure receiver. Hot-gas defrosting can be carried out when the refrigeration system consists of multi-evaporators so that sufficient vapour is generated for defrosting [14].

Hoffenbecker et al. [15] and Dopazo et al. [16] have developed a transient simulation model for predicting heat and mass transfer effects during the hot-gas defrosting cycle. They predicted the time required for complete frost melt. The latter model predicted the time required to defrost is around 14 min. They analysed the effect of refrigerant mass flow rate and inlet temperature, on the defrost time. It was found that the defrosting time increases, and energy supplied decreases as the refrigerant mass flow rate decreases. Hu et al. [17] and Wang et al. [18] carried out an experimental study of various hot-gas defrost methods for an air source transcritical CO₂ heat pump for the water heater. They observed that for the compressor discharge temperature of +60 °C, the

time required to defrost was about 10 min. The heating required for melting the frost was 2659.5 kJ with a defrost efficiency of 41.6–50.84%. Soylemez et al. [19] have reported on a dedicated CO₂ compressor for hot-gas defrosting which utilizes vapour from the cascade condenser to deliver heat to the evaporators in an CO₂-NH₃ cascade system for fishing vessels.

Due to climate concerns, the reintroduction of CO₂ as a refrigerant for both transcritical and cascade refrigeration system has become significant. It can be noted from the literature that various studies on performance of cascade refrigeration systems have been conducted. Along with the freezing, defrosting is also an important process, especially in fish processing units where moisture content is high. Only a few studies are carried out on the defrosting techniques required in cascade deep freezers operating at –40 °C. This paper proposes a mathematical model for CO₂-NH₃ cascade refrigeration system for blast freezers and different hot-gas defrosting configurations that

$$y_{NH_3} = c_1 + c_2 T_{E,cas} + c_3 T_C + c_4 T_{E,cas}^2 + c_5 T_{E,cas} T_C + c_6 T_C^2 + c_7 T_{E,cas}^3 + c_8 T_C T_{E,cas}^2 + c_9 T_{E,cas} T_C^2 + c_{10} T_C^3 \quad (1)$$

can be adopted. In conventional hot-gas defrosting, hot gas from the discharge is redirected to the evaporators. However, in the case of a cascade system, the CO₂ condensing temperature will be in the range of –15 to –5 °C,

$$y_{CO_2} = c_1 + c_2 T_E + c_3 T_{C,cas} + c_4 T_E^2 + c_5 T_E T_{C,cas} + c_6 T_{C,cas}^2 + c_7 T_E^3 + c_8 T_{C,cas} T_E^2 + c_9 T_E T_{C,cas}^2 + c_{10} T_{C,cas}^3 \quad (2)$$

which is not adequate to remove the frost formed on the evaporators. A necessary temperature above 0 °C is required for efficient defrosting. Raising the temperature of the cascade condenser above the freezing point of ice is not a viable solution. Therefore, an analytical study of various defrosting methods such as the prospect of utilizing superheat, existing compressor and dedicated defrost compressor is presented, and the application of each configuration in a blast freezer is explored in this study.

2 System description and mathematical modelling

2.1 Compressor performance

An CO₂-NH₃ cascade refrigeration system with basic components is shown in Fig. 1. The system consists of compressors, a condenser, an expansion device, a low-pressure liquid receiver, and an evaporator for both the high-temperature (HTC) and low-temperature circuits (LTC). The heat is transferred through a cascade plate heat exchanger (PHE) between LTC and HTC. The evaporation of NH₃ and condensation of CO₂ takes place on either side of the cascade plate

heat exchanger (PHE). The cooling is achieved by two 90-kW evaporators.

For HTC circuit Bitzer OSKA7462-K model NH₃ open screw compressor with a displacement volume of 220 m³/h and for LTC circuit Bitzer 4NSL-30 K model CO₂ semi-hermetic reciprocating with a displacement volume of 46.9 m³/h were selected. The compressor performance data based on EN12900 standard is provided by the manufacturer catalogue [20]. This compressor polynomial correlation gives power consumption (*W*), cooling capacity (*W*) and mass flow rate (kg/h) considering 5 K and 10 K superheat for NH₃ and CO₂ compressors respectively. The polynomial coefficient and operating temperature range for both compressors are shown in Table 1.

Using the coefficient from Table 1, the cascade heat exchanger cooling capacity (\dot{Q}_{cas}), compressor power consumption (\dot{W}_H) and mass flow rate (\dot{m}_H) for NH₃ cycle can be determined by substituting in polynomial Eq. (1):

Similarly, freezer evaporator cooling capacity (\dot{Q}_E), compressor power consumption (\dot{W}_L) and mass flow rate (\dot{m}_L) for CO₂ cycle can be determined by substituting in polynomial Eq. (2):

2.2 Thermodynamic analysis

Based on the compressor factory performance data depicted in Section 2.1, the thermodynamic analysis of the cascade system is conducted using Engineering Equation Solver EES[®] which has NH₃ and CO₂ thermophysical property functions build-in. To find the unknown values, the first argument is the name of the refrigerant followed by a minimum of two independent thermodynamic properties such as temperature, pressure, refrigerant quality, enthalpy or entropy. For example temperature = $f(R744, h, P)$ and pressure = $f(R744, T, X)$. The reference according to IIR is 200 kJ/kg and 1 kJ/kg for specific enthalpy and entropy respectively. Considering the state point at each component from Fig. 1, a simplified thermodynamic model has been developed based on the assumptions as follows:

- i. All process including defrosting is at steady state. Heat losses/gains from ambient and pressure drop across the component and pipes are neglected.
- ii. Superheat at the compressor inlet is maintained according to compressor factory data.

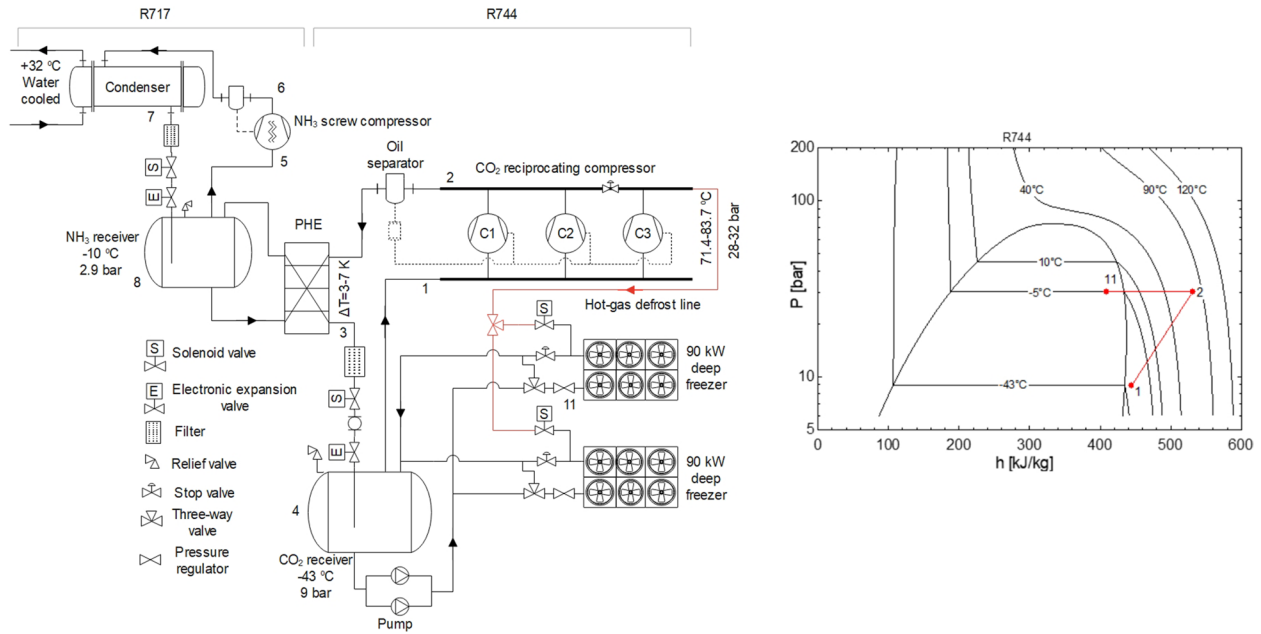


Fig. 1 Schematic and P-h diagram for conventional defrosting (DeConfig0)

Table 1 Coefficients used for compressor polynomial correlation

	c_1	c_2	c_3	c_4	c_5	c_6	c_7	c_8	c_9	c_{10}
NH ₃ ($T_{E,cas} = -20$ to $+12.5$ °C and $T_C = +10$ to $+53$ °C)										
\dot{Q}_{cas}	1.774E+05	3.640E+03	3.572E+03	4.072E+01	1.946E+02	-7.313E+01	1.041E+00	1.353E+00	-2.259E+00	2.016E-01
\dot{W}_H	-1.724E+03	-1.793E+03	2.118E+03	-5.583E+01	8.764E+01	-3.084E+01	-5.243E-01	1.151E+00	-8.737E-01	3.121E-01
\dot{m}_H	4.947E+02	8.475E+00	1.297E+01	7.892E-02	6.888E-01	-1.901E-01	3.314E-03	5.510E-03	-6.602E-03	2.234E-04
CO ₂ ($T_E = -50$ to -15 °C and $T_{C,cas} = -20$ to $+15$ °C)										
\dot{Q}_E	2.863E+05	8.780E+03	-4.178E+03	8.901E+01	-9.986E+01	-1.095E+01	2.718E-01	-6.240E-01	-3.360E-01	1.547E-01
\dot{W}_L	4.299E+03	-1.293E+03	1.410E+03	-2.672E+01	3.209E+01	-2.262E+00	-1.350E-01	1.889E-01	-3.719E-02	-2.309E-02
\dot{m}_L	4.142E+03	1.280E+02	-2.100E+01	1.342E+00	-3.192E-01	-2.121E-01	4.519E-03	-2.178E-04	-5.261E-03	2.321E-03

- iii. Saturated liquid refrigerant is obtained at the outlet of NH₃ condenser and CO₂ cascade condenser.
- iv. Expansion devices undergo isenthalpic expansion.
- v. Isentropic efficiency of 0.75 is assumed for defrost compressor.

The following series of equations are applied on each component; simultaneously, energy and mass balance were verified.

For low-temperature circuit as follows:

CO₂ compressor:

$$\dot{W}_L = \frac{\dot{m}_L}{3600} (h_2 - h_1) \tag{3}$$

Evaporator:

$$\dot{Q}_E = \frac{\dot{m}_L}{3600} (h_1 - h_4) \tag{4}$$

Electronic expansion valve:

$$h_3 = h_4 \tag{5}$$

Cascade heat exchanger temperature difference:

$$T_3 - T_8 = \Delta T \tag{6}$$

where \dot{W}_L , \dot{Q}_E and \dot{m}_L are compressor power input (kW), evaporator cooling capacity (kW) and mass flow rate of CO₂ respectively.

Similarly, for high-temperature circuit as follows:

NH₃ compressor:

$$\dot{W}_H = \frac{\dot{m}_H}{3600}(h_6 - h_5) \quad (7)$$

Condenser:

$$\dot{Q}_C = \frac{\dot{m}_H}{3600}(h_6 - h_7) \quad (8)$$

Electronic expansion valve:

$$h_7 = h_8 \quad (9)$$

Cascade heat exchanger:

$$\dot{Q}_{E,cas} = \frac{\dot{m}_H}{3600}(h_5 - h_8) \quad (10)$$

where \dot{W}_H , \dot{Q}_C and $\dot{Q}_{E,cas}$ are compressor power input (kW), condenser capacity (kW), cascade heat exchanger capacity (kW) and mass flow rate of NH_3 , respectively.

Coefficient of performance (COP) is the scale used to determine the cooling performance, which is given by Eq. (11):

$$COP = \frac{\dot{Q}_E}{\dot{W}_H + \dot{W}_L} \quad (11)$$

The performance of the system (COP) was studied for different condenser temperatures, evaporator temperatures and cascade temperature differences. The fixed values of the operating parameters considered for the thermodynamic analysis are given in Table 2. As per literature [3, 21], the maximum COP depends upon the evaporator, condenser and cascade temperature difference. They have emphasized that COP will be the maximum for an optimal cascade condensing temperature. However, for realistic analysis, compressor factory performance data was used for which the NH_3 evaporating pressure of the cascade heat exchanger was set initially. Therefore, instead of optimum cascade condensing temperature, the cascade evaporating pressure was initialized for maximum COP.

2.3 Hot-gas defrosting criteria

Defrosting is a dynamic process, which is subdivided into different stages such as preheating, frost melting, water draining and dry heating. The dynamics of defrosting have been discussed profoundly in previous literatures [22, 23, 24]. Therefore, in this study, various defrost configurations (DeConfig) required for hot-gas defrosting were focused on considering the total amount of heat (kJ) and CO_2 mass flow rate (kg/h) require to melt the frost. The time taken to melt the frost generally varies from 15 to 30 min in the food processing industry; beyond this, time limit would cause economic loss to the production line [12]. Here, a 90-kW evaporator coil with 1 mm of

Table 2 Fixed values of the operating parameters

Parameters	Values	State points
Condensing temperature of NH_3	+40 (°C)	T_7
Evaporating temperature of CO_2	-43 (°C)	T_4
Cascade heat exchanger temperature difference	5 (K)	ΔT
Cascade heat exchanger evaporating pressure	2.9 (bar)	P_5
Cooling capacity	90 (kW)	

frost deposit is considered for defrosting. The evaporator is made ready for defrosting by shutting off the liquid CO_2 supply first. The evaporator outlet valve is kept open for 180 to 400 s, with evaporator fans in a running state to boil off residual liquid CO_2 . Then, the evaporator fans are switched off, and the solenoid valve for the hot-gas bypass is opened. After defrosting is completed, the hot-gas bypass solenoid is closed. At last, liquid CO_2 feed to the evaporator is opened, and evaporator fans are restarted [25]. The amount of heat required to melt the frost is depicted in Table 3.

DeConfig0 shown in Fig. 1 is a basic conventional method used for hot-gas defrosting. The schematic layout and p-h diagram of newly proposed defrost configurations are shown in Figs. 2, 3, 4 and 5. Throughout the analysis, one evaporator is on cooling, and the other will undergo defrosting so that a constant supply of hot gas is obtained. In DeConfig0, hot gas from CO_2 compressor discharge is redirected to the evaporator by the opening of a solenoid valve. Superheated vapour from the compressor discharge is utilized for defrosting because the saturation temperature at the cascade condenser is lower than 0 °C. Management of condensed liquid CO_2 from the evaporator after the defrosting could be avoided; on the other hand, the mass flow rate of hot gas will be high which is impractical for the NH_3 refrigerant but feasible for CO_2 refrigerant because of its comparatively low specific volume. In DeConfig1 (Fig. 2), one of the multi-compressor is used to elevate the pressure and temperature of hot gas above the cascade condenser saturation temperature so that latent heat can also be utilized for defrosting. A stop valve is used to block discharge from the main compressor, and the suction vapour is compressed above cascade condenser pressure so that temperature above the melting point of ice is obtained. The condensed CO_2 after melting the frost is throttled through a pressure regulator valve and collected in the liquid receiver. In DeConfig2 (Fig. 3), an additional defrost compressor is installed where the discharge hot gas from the CO_2 compressor is fed into the suction of defrost compressor. Here, the hot-gas pressure and temperature are elevated above the saturation pressure of the cascade condenser to a maximum temperature of +10 °C. The hot gas will reject heat to melt the frost deposit, and condensed CO_2 is collected in the liquid receiver after throttling through

Table 3 Defrosting criteria [26]

Parameter	Value	Units
Frost thickness	1	mm
Evaporator cooling capacity	90	kW
Frost density	300	kg/m ³
Surface area of evaporator	450	m ²
Mass of ice	135	kg
Specific heat of ice	2.1	kJ/kg K
Specific heat of water	4.2	kJ/kg K
Latent heat of fusion	336	kJ/kg
Start temperature	-43	°C
End temperature	+10	°C
Heat required for defrosting	60,000	kJ

the pressure regulator valve. In DeConfig3a (Fig. 4), the existing compressor among the multi-compressor can be used as defrost compressor for batch process defrosting in the case of a blast freezer. To maintain the compressor in its operating temperature envelope and to have stable lubrication, an internal heat exchanger (IHX) or desuperheater (DSH) is required between the discharge of the main refrigeration compressor and the suction of defrost compressor. By using ambient temperature or return condensed CO₂, the hot gas can be cooled before entering into defrost compressor, but not near to the saturation temperature. Alternatively, desuperheating of hot gas can also be achieved from the cascade condenser for controlled cooling of the hot gas as shown in DeConfig3b (Fig. 5). The choice of either configuration depends on the selection of

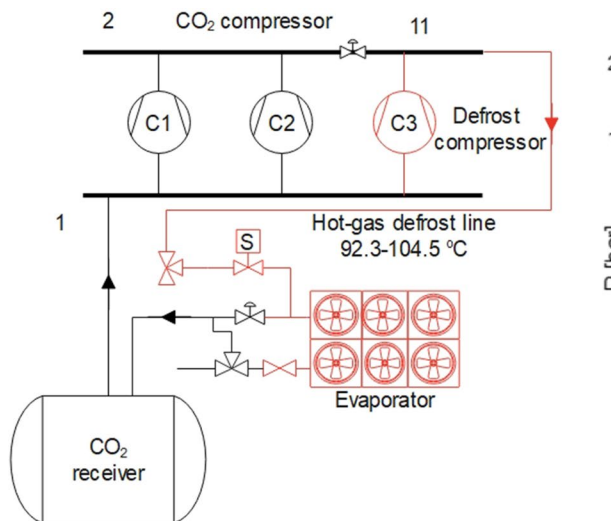


Fig. 2 DeConfig1 and P-h diagram

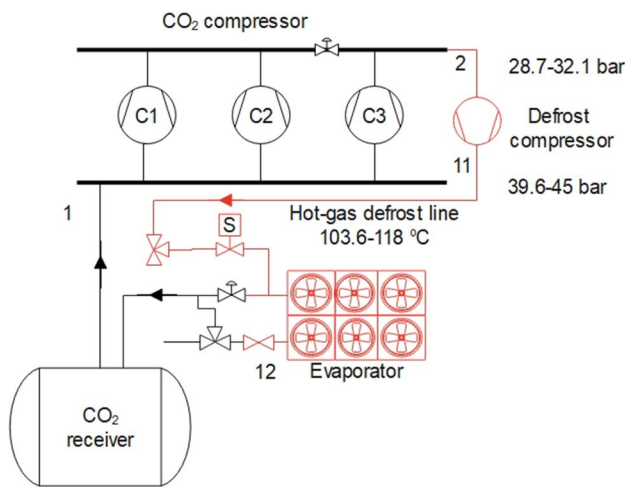


Fig. 3 DeConfig2 and P-h diagram

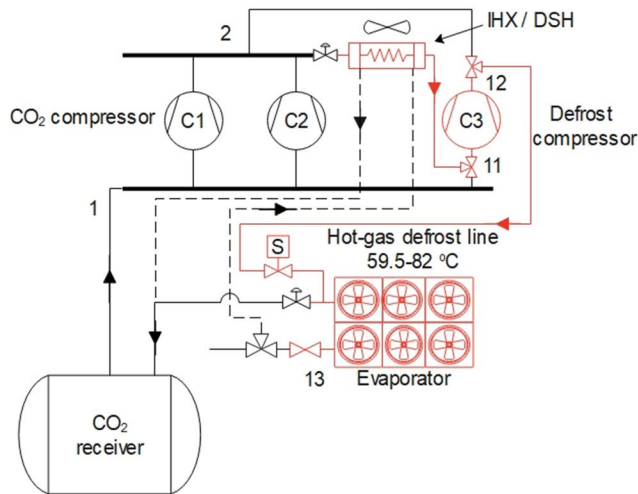


Fig. 4 DeConfig3a and P-h diagram

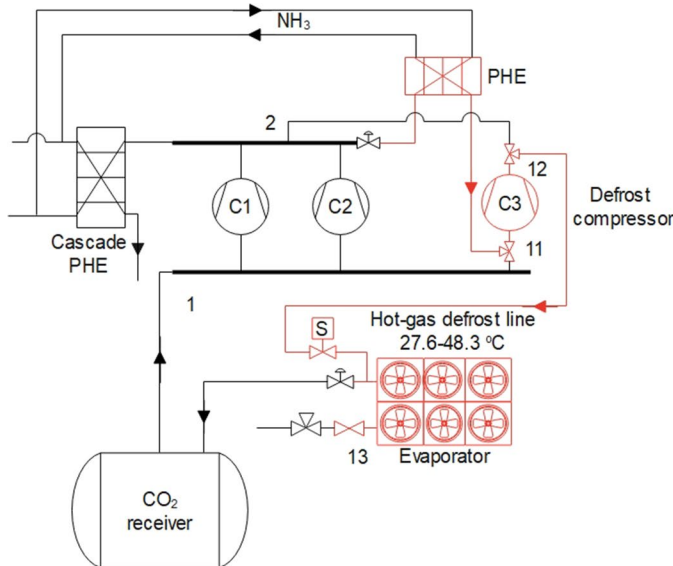


Fig. 5 DeConfig3b and P-h diagram

the compressor and its operating parameters as the same compressor is used for refrigeration and defrosting. Therefore, drastic changes in the compressor capacity can be avoided.

The defrost compressor work input for DeConfig1, DeConfig2 and DeConfig3a and DeConfig3b is expressed in Eqs. (12), (13), (14) and (15) respectively.

$$\dot{W}_{de} = \dot{m}_{hotgas}(h_{11} - h_1) \tag{12}$$

$$\dot{W}_{de} = \dot{m}_{hotgas}(h_{11} - h_2) \tag{13}$$

$$\dot{W}_{de} = \dot{m}_{hotgas}(h_{12} - h_{11}) \tag{14}$$

$$\dot{W}_{de} = \dot{m}_{hotgas}(h_{12} - h_{11}) \tag{15}$$

The defrosting configurations are evaluated and compared by its defrosting efficiency. For numerical analysis, defrost efficiency can be defined as the ratio of amount energy required to melt the frost deposit, to the total energy consumed by the compressors.

$$\eta_{de} = \frac{\dot{Q}_{de}}{\dot{W}_H + \dot{W}_L + \dot{W}_{de}} \tag{16}$$

Table 4 Exergy equation for defrosting components

Components	Equations
Defrosting compressor	$\dot{E}x_{des} = T_0(\dot{m}_{hotgas}(s_{in} - s_{out}))$ (17)
Desuperheater	$\dot{E}x_{des} = T_0(\dot{m}_{hotgas}(s_{in} - s_{out}) - \frac{\dot{Q}_{dsh}}{T_{dsh}})$ (18)
Cascade desuperheater	$\dot{E}x_{des} = T_0(\dot{m}_{hotgas}(s_{in} - s_{out}) + \dot{m}_H(s_{in} - s_{out}))$ (19)
Defrosting evaporator	$\dot{E}x_{des} = T_0(\dot{m}_{hotgas}(s_{in} - s_{out}) - \frac{\dot{Q}_{de}}{T_{de}})$ (20)

2.4 Exergy analysis

The exergy analysis for defrosting is carried out on the components involved in defrosting such as defrosting compressor, desuperheater and evaporator under defrosting. Total system exergy analysis has been conducted in previous literatures; therefore, it is not focused in this section [27]. The chemical, kinetic and potential exergies are neglected; thus, at a state point, the physical exergy of the system for the defrosting compressor, desuperheater and defrosting evaporator is shown in Eqs. (17), (18), (19) and (20), respectively, presented in Table 4.

where $\dot{E}x_{des}$ is the exergy destruction/lost, T_0 is the ambient temperature in K and \dot{Q}_{dsh} and \dot{Q}_{de} are the desuperheater capacity and heat required for defrosting respectively in W. The outlet temperature of desuperheater and defrosting evaporator coil is denoted by T_{dsh}

and T_{de} in K. The change in entropy is termed as s_{in} and s_{out} across the component under analysis.

3 Model validation

The mathematical model for the cascade system was validated with previous literatures [4, 7, 10]. For the analysis, one evaporator was in refrigeration mode, and the other evaporator was in defrosting mode so that a continuous supply of hot gas is obtained. The maximum COP of refrigeration that depends on optimum cascade condensing temperature was compared and validated as shown in Table 5. The maximum deviation in percentage when compared to the published data, Saini et al. [10], Lee et al. [4] and Dopazo and Fernández-Seara [7], is 5.1%, 7.9% and 13.6%, respectively. The present cascade refrigeration model shows a good agreement with previously developed thermodynamic models. Therefore, as the baseline mathematical model deviation is in the acceptable range, the defrosting analysis can be considered valid.

4 Results and discussion

In this study, the cascade heat exchanger evaporating pressure was analysed first. A constant value of evaporating pressure was fixed for a particular condenser outlet

Table 5 COP comparison between present and published studies

T_E (°C)	T_C (°C)	ΔT (K)	$T_{C,cas}$ (°C)	COP	Deviation (%)
Present study					
-45	30	3	-10.6	1.4	-
-45	35	3	-8.8	1.29	-
-45	40	3	-7	1.18	-
-45	30	5	-8.6	1.34	-
-45	35	5	-6.8	1.23	-
-45	40	5	-5.1	1.12	-
-40	35	5	-6.8	1.38	-
-50	35	5	-8.6	1.1	-
Lee et al. [4]					
-45	30	3	-17	1.51	7.9
-45	35	3	-15	1.38	7.0
-45	40	3	-13	1.25	5.9
-45	30	5	-15	1.44	7.5
-45	35	5	-13	1.31	6.5
-45	40	5	-11	1.2	7.1
Dopazo and Fernández-Seara [7]					
-40	35	5	-10.3	1.42	2.9
-45	35	5	-13.3	1.14	7.3
-50	35	5	-15.8	0.95	13.6
Saini et al. [10]					
-40	35	5	-10.5	1.45	5.1
-45	35	5	-12.4	1.29	4.9
-50	35	5	-14.7	1.14	3.6

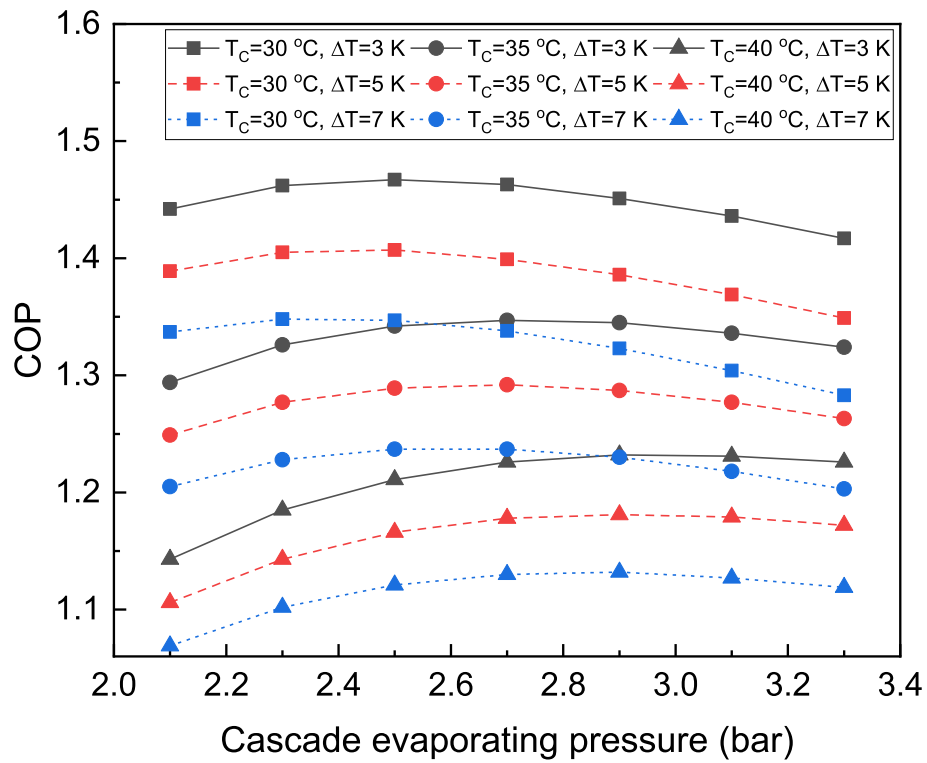


Fig. 6 Variation of system performance with cascade evaporating pressure

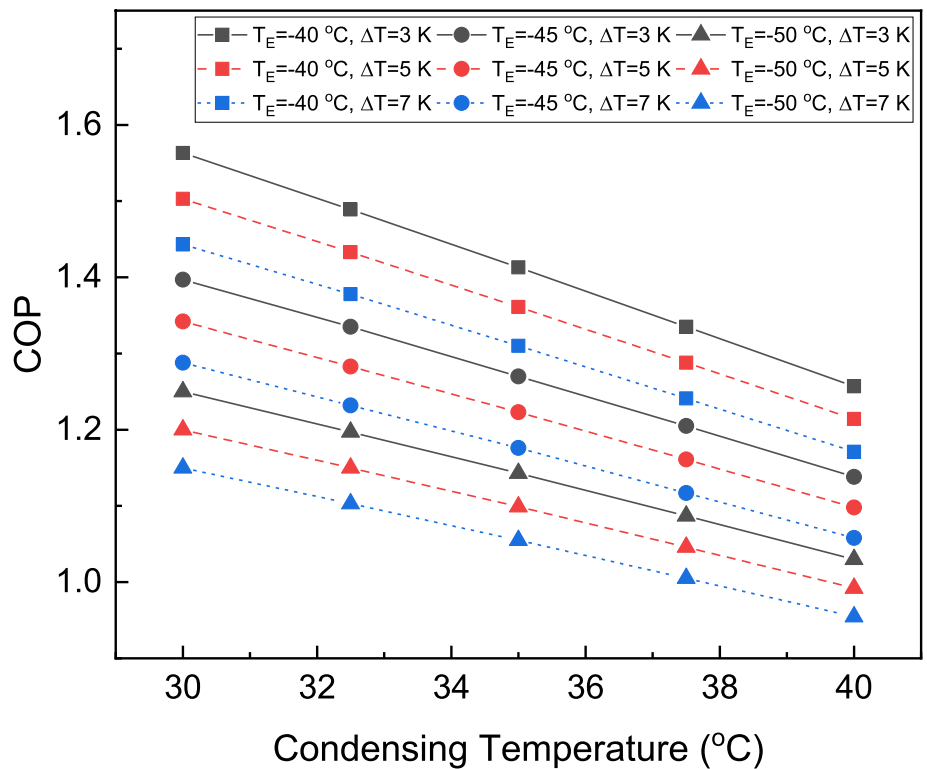


Fig. 7 Variation of system performance with condensing temperature

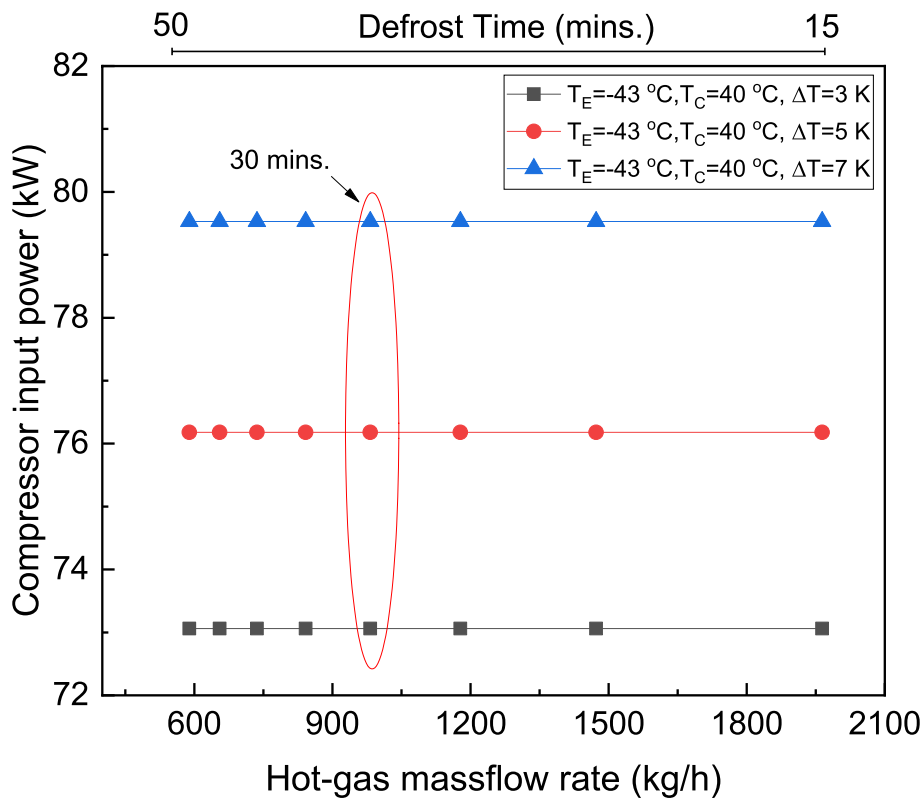


Fig. 8 Total power consumption of baseline unit showing time required for defrosting

temperature for all defrost configurations. Secondly, the effect of operating parameters such as evaporating temperature T_E , condensing temperature T_C and cascade temperature difference ΔT on COP was depicted. Hereafter, the additional power consumed in different defrost configurations (DeConfig) was discussed.

4.1 Initialization of cascade heat exchanger evaporating pressure

The study was carried out using compressor factory performance data, for which the evaporating and condensing temperature for both circuits have to be decided initially. The parameters that need to be initialized were evaporator temperature, condenser outlet temperature and cascade temperature difference. For this, the cascade evaporating positive pressure had to be fixed. However, it was observed that by variation of cascade evaporating pressure, the COP of the system reaches a peak value and then declines as shown in Fig. 6. It can be seen that for a condensing temperature of +40 °C and evaporating temperature of -43 °C, the maximum COP obtained were 1.23, 1.18 and 1.13 for cascade temperature difference of 3 K, 5 K and 7 K respectively against nearby value of 2.9 bar cascade evaporating pressure.

4.2 Effect T_C , T_E and ΔT on system performance

Figure 7 shows the effect of condensing temperature T_C on COP for various evaporating temperature T_E of -40 °C, -45 °C and -50 °C and cascade temperature difference ΔT of 3 K, 5 K and 7 K, respectively. In Fig. 7, the COP decreases with an increase in condensing temperature and a drop in evaporating temperature. COP is linearly related to the operating parameters of T_C , T_E and ΔT . These are expected trends, because, when the NH_3 condensing temperature increases, compressor power consumption will increase with rise in pressure ratio. When ΔT is large, the performance of the cascade system reduces for an invariant cooling capacity, T_C and T_E , because of the increase in entropy, resulting in more irreversibility of the refrigeration cycle. Consequently, the COP of the cascade system decreases. For a high condensing temperature of +40 °C, COP values between 0.95 and 1.25 are obtained for different operating parameters as shown in Fig. 7.

4.3 Analysis of different defrost configurations

The energy consumption required for defrosting by the individual compressor was investigated for various cascade temperature differences ΔT of 3 K, 5 K and 7 K and discharge pressure of defrosting compressor P_{de} of 39 bar

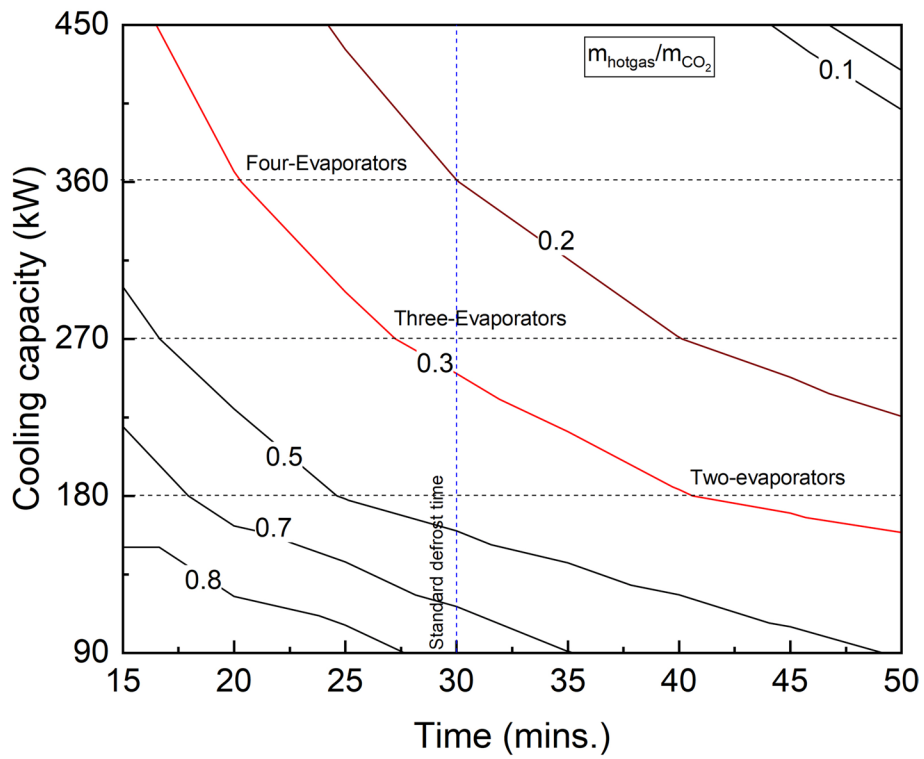


Fig. 9 Number of evaporators required for conventional defrosting

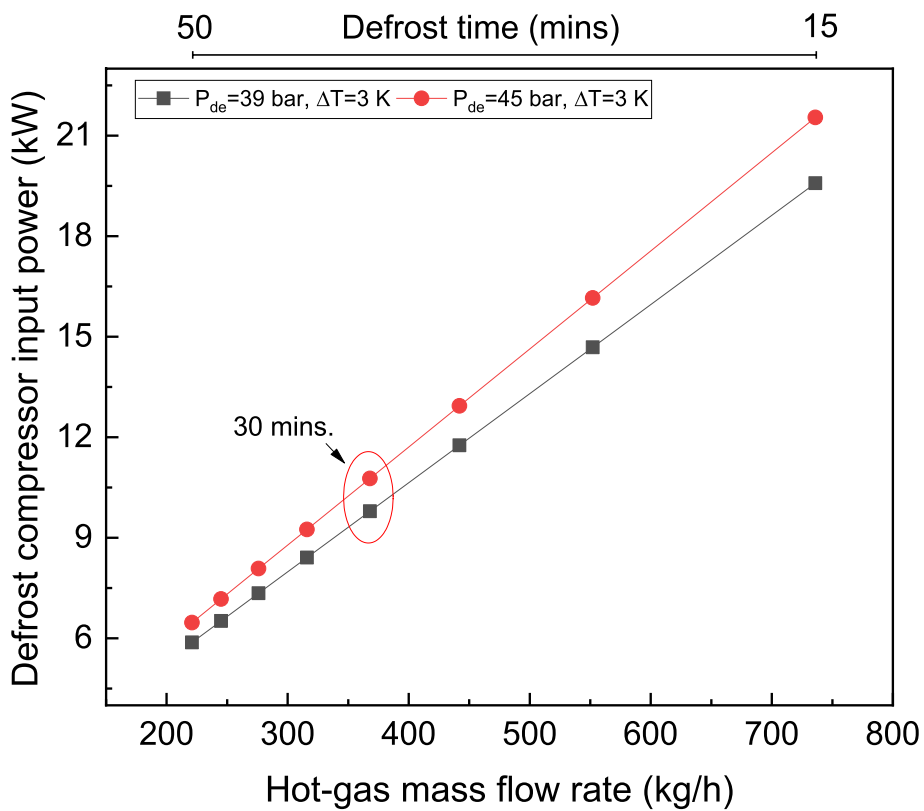


Fig. 10 Variation of W_{de} with hot-gas mass flow rate for DeConfig1

and 45 bar with respect to different hot-gas mass flow rates \dot{m}_{hotgas} .

In DeConfig0 as shown in Fig. 8, the energy consumed by the system for different cascade temperature differences is 73.06, 76.18 and 79.53 kW. This shows the total power consumption of the baseline system. In this case, the superheat from the main compressor is utilized for defrosting. It is evident that a high mass flow rate of 982 kg/h is required for a standard duration of defrosting which is not feasible for a system with single or two evaporators. This configuration can be adopted only for multi-evaporators as shown in Fig. 9, which represents the number of 90-kW evaporators required in terms of cooling capacity for various defrosting time duration from 15 to 50 min. For a defrosting time up to 30 min and a hot-gas extraction ratio of 0.3, more than three evaporators are required to obtain sufficient hot gas for defrosting. In this figure, hot-gas extraction ratio is represented by the ratio of mass flow rate of hot gas by mass flow rate of mainline CO₂ refrigerant. An increase in the extraction ratio will result in an inadequate supply of refrigerant to the cooling evaporators.

In DeConfig1 as shown in Fig. 10, the power consumption by defrost compressor increases linearly for various

mass flow rates from 221 to 736 kg/h. For a mass flow rate of 316 kg/h, the power consumed is 8.40 and 9.24 kW for discharge pressure of 39 and 45 bar respectively. The effect of cascade temperature difference is negligible in this configuration as the suction vapours are supplied to the defrost compressor.

In DeConfig2 as shown in Fig. 11, similar to the previous case, the power consumption by defrost compressor increases linearly for various mass flow rates ranging from 212 to 707 kg/h. For a mass flow rate of 353 kg/h and defrost compressor discharge pressure of 45 bar, 2.80–3.62 kW of power is consumed for different cascade temperature differences as the hot gas from the main compressor discharge is directly supplied to defrost compressor suction. Highly superheated hot gas is available for defrosting; therefore, the defrosting compressor power consumption is low. However, the stability of lubricating oil and operating temperature envelop of defrost compressor should be supervised. Even though the total power consumption of the system is high for higher cascade temperature differences, the power consumed for defrosting is low due to the rise in cascade condensing temperature.

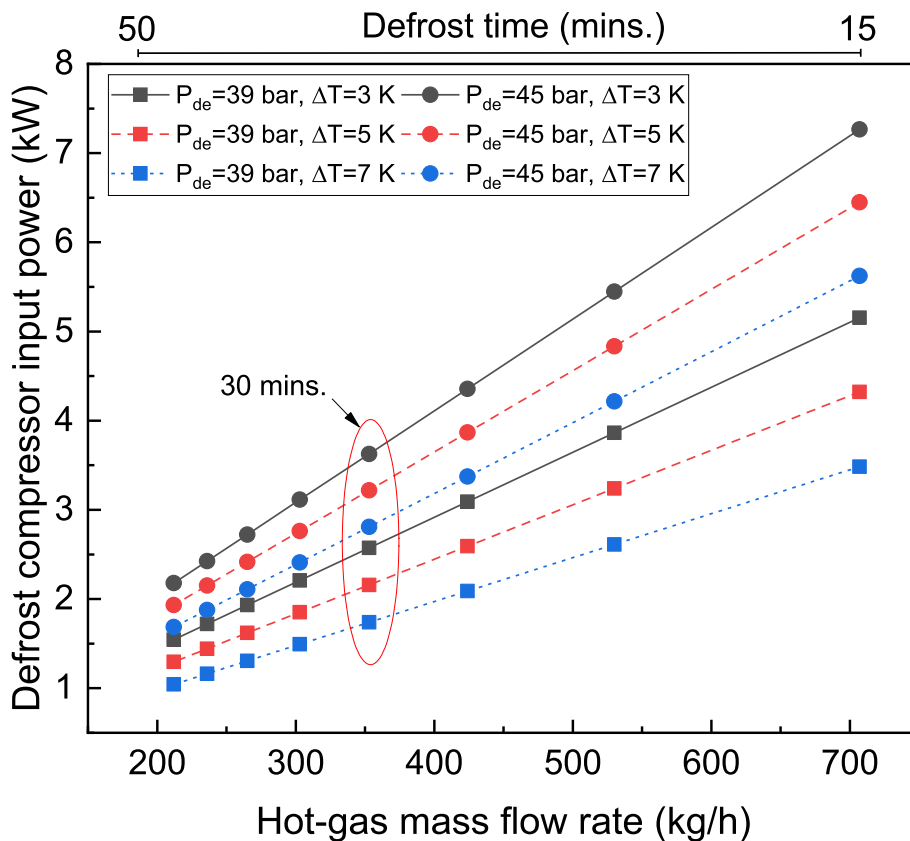


Fig. 11 Variation of W_{de} with hot-gas mass flow rate for DeConfig2

Figures 12 and 13 illustrates the power consumed for defrosting of DeConfig3a and DeConfig3b respectively. In DeConfig3a, the hot gas is desuperheated before entering the defrost compressor. One of the main compressors is modified to operate as defrost compressor, which should have a wide operating temperature envelope. Similarly, for DeConfig3b where the modified defrost compressor with narrow operative temperature envelope compared to DeConfig3a, a plate heat exchanger connected to the cascade evaporator can be used to reduce the hot-gas temperature to an acceptable level. According to Figs. 12 and 13, at defrost discharge pressure of 45 bar, for a mass flow rate of 425 kg/h and 470 kg/h, 2.62–3.59 kW and 6.68–6.88 kW of energy is consumed for DeConfig3a and DeConfig3b respectively. It can be deduced that to maintain lubricant oil stability, the hot gas can be desuperheated, where the defrost compressor power consumption is less. However, refrigeration/defrosting compressors should have a wide operating range.

The defrosting efficiency comparison of all four configurations for different cascade temperature differences and defrosting time of 30 min are depicted in Fig. 14. For all data set, average defrosting efficiency of 43.8%, 38.5%, 42.5%, 42%, and 39.7% was achieved for DeConfig0, DeConfig1, DeConfig2, DeConfig3a, and DeConfig3b

respectively. DeConfig0 shows the highest defrosting efficiency because no additional energy is consumed for defrosting. Moreover, for all configurations, the efficiency remains in an average range of 38.5–43.8% which is in accordance with previous literatures where defrosting efficiency is reported in the range of 30–40% for hot-gas bypass defrosting for transcritical CO₂ heat pumps [17, 18].

4.4 Effect of ΔT on defrosting exergy

Figure 15 depicts the influence of cascade temperature difference on the exergy lost for defrosting components such as defrosting compressor, desuperheater, cascade desuperheater, and defrosting evaporator. From the energy analysis in the previous Section 4.3, it is observed that cascade temperature differences have an influence on the defrosting energy consumption. For fixed operating conditions of heat required for defrosting, under which the elevated defrosting pressure of 45 bar and temperature of +10 °C, the condensing temperature is +40 °C for an ambient temperature of +35 °C, and the exergy lost for different defrost configurations is shown in Fig. 15. It is obvious that exergy destruction is maximum for DeConfig0 because of high mass flow rate of

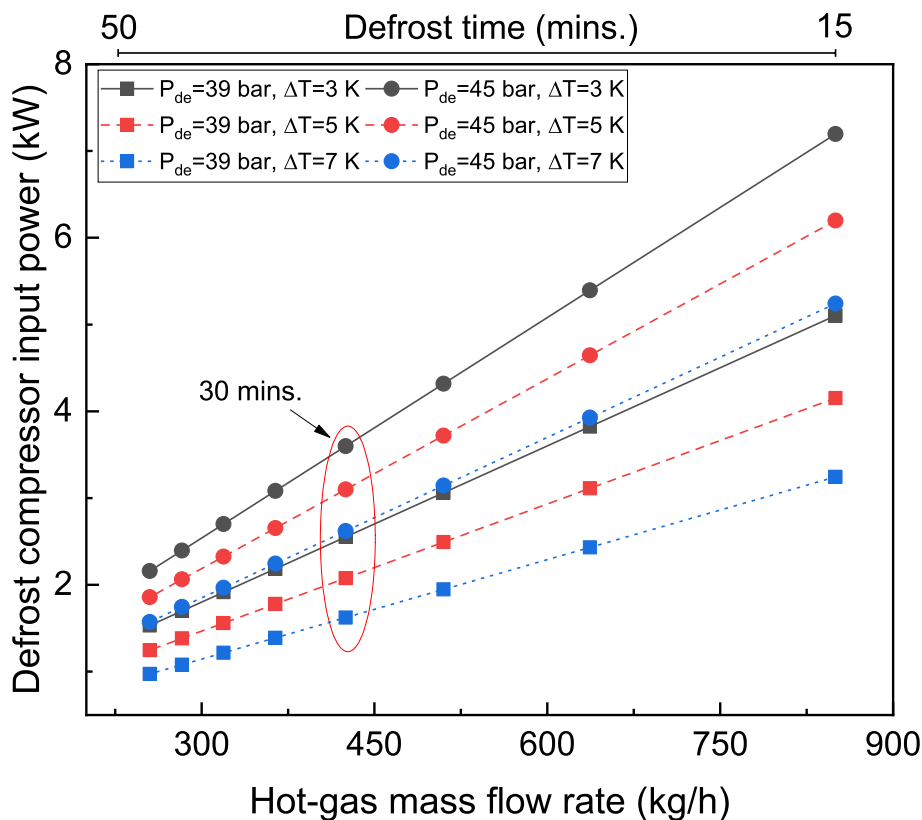


Fig. 12 Variation of W_{de} with hot-gas mass flow rate for DeConfig3a

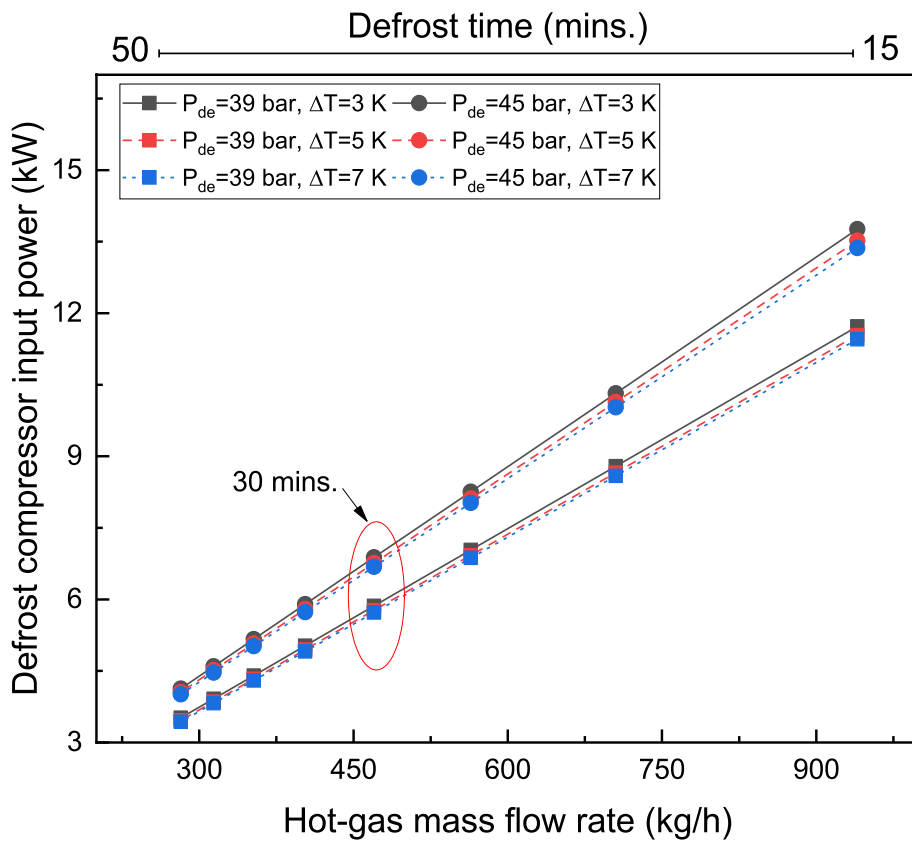


Fig. 13 Variation of W_{de} with hot-gas mass flow rate for DeConfig3b

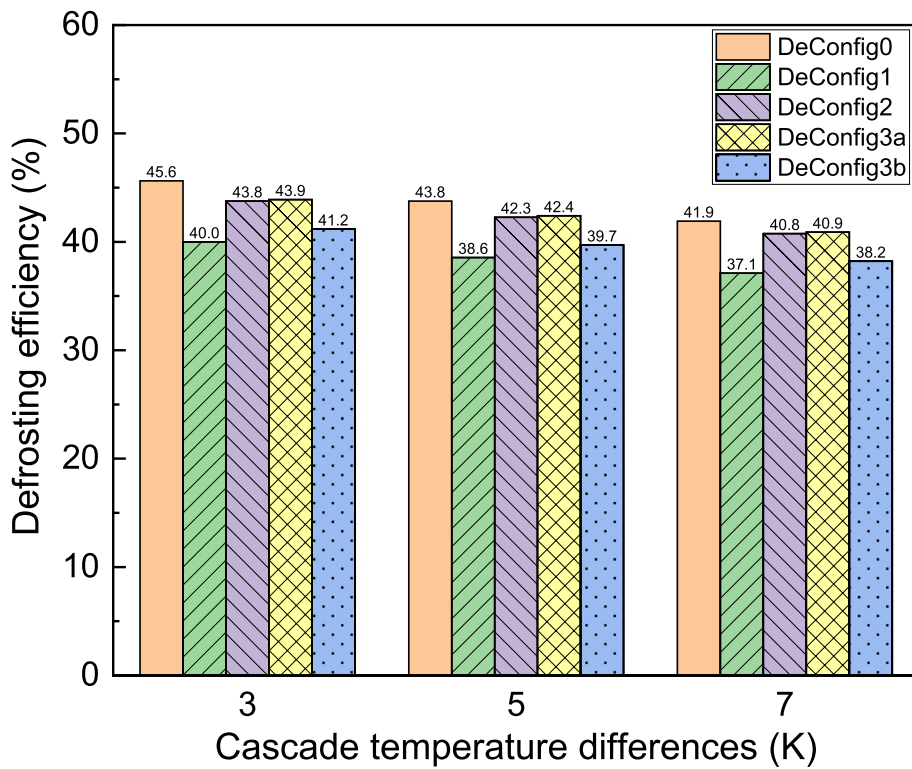


Fig. 14 Defrosting efficiency of various DeConfig

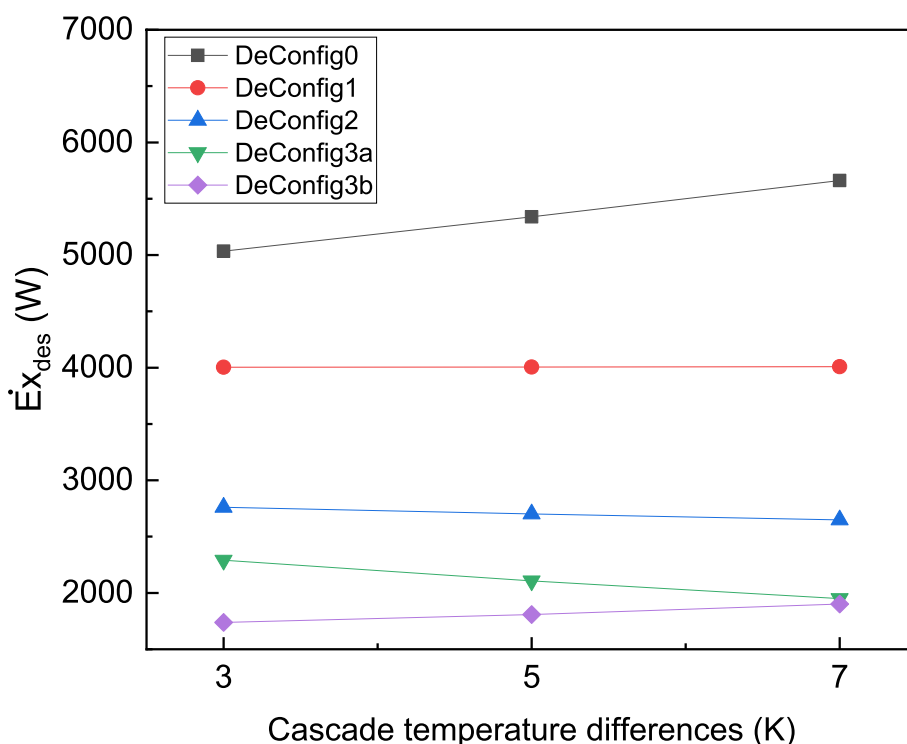


Fig. 15 Exergy destruction for various defrosting configurations

superheated vapour. DeConfig3b shows the lowest exergy destruction.

5 Conclusions

Four hot-gas defrosting configurations for CO₂-NH₃ cascade refrigeration system for a blast freezer commonly used in seafood industry were investigated in this study. The main difference between these configurations was the arrangement of the defrosting compressor, and the additional energy consumptions required for the systems were numerically simulated. The DeConfig0 utilized high mass flow rate hot-gas superheat which is the conventional method adopted for defrosting. However, this configuration can be adopted for a centralized cascade refrigeration system with more than three evaporators so that an adequate supply of refrigerant for simultaneous cooling and hot-gas defrosting is obtained. For small-scale deep freezers, an additional defrosting compressor is required. When suction vapours are compressed above the saturation pressure and temperature of the cascade condenser, defrosting compressor (DeConfig1) consumed high energy in the range of 8.4–9.2 kW. An alternative to reduce the additional energy consumption, hot gas from the main compressor discharge was supplied to the defrosting compressor. The least energy demanding alternative was DeConfig2, which was in the range of 2.8–3.6 kW, where a dedicated

compressor was used. Additionally, to reduce the cost of additional compressors, DeConfig3a and DeConfig3b can be selected where defrosting energy consumption was in the range of 2.6–3.6 kW and 6.7–6.9 kW, respectively. The lubricating oil stability was maintained by de-superheating the hot gas which depends on the operating temperature envelop of the compressors. For wide operating range compressor, DeConfig3a and for narrow operating range compressor, DeConfig3b configuration is recommended.

6 Nomenclature

COP	coefficient of performance
DeConfig	defrost configurations
DSH	desuperheater
\dot{E}_x	Exergy (W)
h	enthalpy (kJ/kg)
HTC	high temperature circuit
IHX	internal heat exchanger
LTC	low temperature circuit
\dot{m}	mass flow rate (kg/h)
P	pressure (bar)
\dot{Q}	amount of heat (W)
s	entropy (J/K)
T	temperature (°C)
\dot{W}	power input (W)
ΔT	cascade temperature difference (K)

6.1 Greek symbol

η efficiency (%)

6.2 Subscripts

C condensing
 cas cascade
 de defrost compressor
 des destruction
 dsh desuperheater
 E evaporating
 H high temperature
 hotgas CO₂ hot-gas
 L low temperature

Acknowledgements

The authors acknowledge the support received from the Indo-Norwegian project "Future Refrigeration India: INDEE+" (CIFT/FRI-INDEE 2021) funded by the Norwegians Ministry of Foreign Affairs, coordinated by Norwegian University of Science and Technology and SINTEF Ocean, Norway.

Authors' contributions

BSA, conceptualization, methodology, and writing—original draft preparation. SK, software. MS, validation. GN, supervision. MS, supervision. VS, software and validation. MSD, writing—reviewing and editing. SKK, writing—reviewing and editing. AH, project administration. KNW, resources and analysis tools.

Funding

The author(s) acknowledge the funding received from the Indo-Norwegian project "Future Refrigeration India: INDEE+" (CIFT/FRI-INDEE 2021) funded by the Norwegians Ministry of Foreign Affairs, coordinated by Norwegian University of Science and Technology and SINTEF Ocean, Norway.

Availability of data and materials

All the data is available in the manuscript.

Declarations

Competing interests

The authors declare that they have no competing interests.

Author details

¹Engineering Section, ICAR-Central Institute of Fisheries Technology, Cochin 682029, India. ²Centre for Water Resources Development and Management, Kozhikode 673571, India. ³School of Energy Science and Engineering, Indian Institute of Technology, Kharagpur 721302, India. ⁴Department of Mechanical Engineering, Birla Institute of Technology and Science, Pilani 333031, India. ⁵Department of Energy and Process Engineering, Norwegian University of Science and Technology, Trondheim 7034, Norway. ⁶Fisheries and New Biomarine Industry, SINTEF Ocean AS, Trondheim 7465, Norway.

Received: 18 July 2023 Accepted: 30 January 2024

Published online: 28 February 2024

References

- NFBD (2023). National Fisheries Development Board, Department of Fisheries, Ministry of Fisheries, Animal husbandry & Dairying, Govt. of India. Available at: https://nfdb.gov.in/welcome/about_indian_fisheries. viewed on 15/07/2023
- Pan, M., Zhao, H., Liang, D., Zhu, Y., Liang, Y., & Bao, G. (2020). A review of the cascade refrigeration system. *Energies*, 13(9). <https://doi.org/10.3390/en13092254>
- Bingming, W., Huagen, W., Jianfeng, L., & Ziwen, X. (2009). Experimental investigation on the performance of NH₃/CO₂ cascade refrigeration system with twin-screw compressor. *International Journal of Refrigeration*, 32(6), 1358–1365. <https://doi.org/10.1016/j.ijrefrig.2009.03.008>
- Lee, T. S., Liu, C. H., & Chen, T. W. (2006). Thermodynamic analysis of optimal condensing temperature of cascade-condenser in CO₂/NH₃ cascade refrigeration systems. *International Journal of Refrigeration*, 29(7), 1100–1108. <https://doi.org/10.1016/j.ijrefrig.2006.03.003>
- Getu, H. M., & Bansal, P. K. (2008). Thermodynamic analysis of an R744–R717 cascade refrigeration system. *International Journal of Refrigeration*, 31(1), 45–54. <https://doi.org/10.1016/j.ijrefrig.2007.06.014>
- Alberto Dopazo, J., Fernández-Seara, J., Sieres, J., & Uhiá, F. J. (2009). Theoretical analysis of a CO₂-NH₃ cascade refrigeration system for cooling applications at low temperatures. *Applied Thermal Engineering*, 29(8–9), 1577–1583. <https://doi.org/10.1016/j.applthermaleng.2008.07.006>
- Dopazo, J. A., & Fernández-Seara, J. (2011). Experimental evaluation of a cascade refrigeration system prototype with CO₂ and NH₃ for freezing process applications. *International Journal of Refrigeration*, 34(1), 257–267. <https://doi.org/10.1016/j.ijrefrig.2010.07.010>
- Yilmaz, B., Mancuhan, E., & Erdonmez, N. (2018). A parametric study on a subcritical CO₂/NH₃ cascade refrigeration system for low temperature applications. *Journal of Solar Energy Engineering, Transactions of the ASME*, 140(9), 1–7. <https://doi.org/10.1115/1.4039976>
- Bellos, E., & Tzivanidis, C. (2019). A theoretical comparative study of CO₂ cascade refrigeration systems. *Applied Sciences (Switzerland)*, 9(4). <https://doi.org/10.3390/app9040790>
- Saini, S. K., Dasgupta, M. S., Widell, K. N., & Bhattacharyya, S. (2021). Comparative analysis of a few novel multi-evaporator CO₂-NH₃ cascade refrigeration system for seafood processing & storage. *International Journal of Refrigeration*, 131(January), 817–825. <https://doi.org/10.1016/j.ijrefrig.2021.07.017>
- Klingebiel, J., Hassan, M., Venzik, V., Vering, C., & Müller, D. (2023). Efficiency comparison between defrosting methods: A laboratory study on reverse-cycle defrosting, electric heating defrosting, and warm brine defrosting. *Applied Thermal Engineering*, 233(May), 121072. <https://doi.org/10.1016/j.applthermaleng.2023.121072>
- Amer, M., & Wang, C. C. (2017). Review of defrosting methods. *Renewable and Sustainable Energy Reviews*, 73(October 2016), 53–74. <https://doi.org/10.1016/j.rser.2017.01.120>
- Xi, Z., Yao, R., Li, J., Du, C., Yu, Z., & Li, B. (2021). Experimental studies on hot gas bypass defrosting control strategies for air source heat pumps. *Journal of Building Engineering*, 43(May), 103165. <https://doi.org/10.1016/j.jobbe.2021.103165>
- Bansal, P. K., & Jain, S. (2007). Cascade systems: Past, present, and future. *ASHRAE Transactions*, 113 PART 1, 245–252.
- Hoffenbecker, N., Klein, S. A., & Reindl, D. T. (2005). Hot gas defrost model development and validation. *International Journal of Refrigeration*, 28(4), 605–615. <https://doi.org/10.1016/j.ijrefrig.2004.08.016>
- Dopazo, J. A., Fernandez-Seara, J., Uhiá, F. J., & Diz, R. (2010). Modelling and experimental validation of the hot-gas defrost process of an air-cooled evaporator. *International Journal of Refrigeration*, 33(4), 829–839. <https://doi.org/10.1016/j.ijrefrig.2009.12.027>
- Hu, B., Yang, D., Cao, F., Xing, Z., & Fei, J. (2015). Hot gas defrosting method for air-source transcritical CO₂ heat pump systems. *Energy and Buildings*, 86, 864–872. <https://doi.org/10.1016/j.enbuild.2014.10.059>
- Wang, Y., Ye, Z., Song, Y., Yin, X., & Cao, F. (2020). Experimental investigation on the hot gas bypass defrosting in air source transcritical CO₂ heat pump water heater. *Applied Thermal Engineering*, 178(June), 115571. <https://doi.org/10.1016/j.applthermaleng.2020.115571>
- Söylemez, E., Widell, K. N., Gabriellii, C. H., Ladam, Y., Lund, T., & Hafner, A. (2022). Overview of the development and status of carbon dioxide (R-744) refrigeration systems onboard fishing vessels. *International Journal of Refrigeration*, 140, 198–212. <https://doi.org/10.1016/j.ijrefrig.2022.05.007>
- Bitzer software (2023). Version 6.18. <https://www.bitzer.de/websoftware/>. Accessed 15 July 2023
- Aghazadeh Dokandari, D., Setayesh Hagh, A., & Mahmoudi, S. M. S. (2014). Thermodynamic investigation and optimization of novel ejector-expansion CO₂/NH₃ cascade refrigeration cycles (novel CO₂/NH₃ cycle). *International Journal of Refrigeration*, 46(94), 26–36. <https://doi.org/10.1016/j.ijrefrig.2014.07.012>
- Badri, D., Toublanc, C., Rouaud, O., & Havet, M. (2021). Review on frosting, defrosting and frost management techniques in industrial food freezers.

- Renewable and Sustainable Energy Reviews*, 151(January), 111545. <https://doi.org/10.1016/j.rser.2021.111545>
23. Huang, D., Li, Q., & Yuan, X. (2009). Comparison between hot-gas bypass defrosting and reverse-cycle defrosting methods on an air-to-water heat pump. *Applied Energy*, 86(9), 1697–1703. <https://doi.org/10.1016/j.apenergy.2008.11.023>
 24. Song, M., Deng, S., Dang, C., Mao, N., & Wang, Z. (2018). Review on improvement for air source heat pump units during frosting and defrosting. *Applied Energy*, 211(December 2017), 1150–1170. <https://doi.org/10.1016/j.apenergy.2017.12.022>
 25. Stoecker, W. F., Lux, J. J., & Kooy, R. J. (1983). Energy considerations in hot-gas defrosting of industrial refrigeration coils. *ASHRAE Transactions*, 89(pt 2A 2B), 549–573.
 26. Thermofin (2023). Thermofin heat exchangers Germany, Blast freezers, TOFL model for CO₂. Available at: <https://www.thermofin.de/en/blast-freezers-evaporators.php>. viewed on 15/07/2023
 27. Gholamian, E., Hanafizadeh, P., & Ahmadi, P. (2018). Advanced exergy analysis of a carbon dioxide ammonia cascade refrigeration system. *Applied Thermal Engineering*, 137, 689–699. <https://doi.org/10.1016/j.applthermaleng.2018.03.055>

Publisher's Note

Springer Nature remains neutral with regard to jurisdictional claims in published maps and institutional affiliations.